Check for updates

SUPERNOVAE

Emission lines due to ionizing radiation from a compact object in the remnant of Supernova 1987A

C. Fransson[1]*, M. J. Barlow[2]†, P. J. Kavanagh[3,4]†, J. Larsson[5]†, O. C. Jones[6], B. Sargent[7,8], M. Meixner[9], P. Bouchet[10], T. Temim[11], G. S. Wright[6], J. A. D. L. Blommaert[12], N. Habel[9], A. S. Hirschauer[7], J. Hjorth[13], L. Lenkić[14], T. Tikkanen[15], R. Wesson[16], A. Coulais[10,17], O. D. Fox[7], R. Gastaud[18], A. Glasse[6], J. Jaspers[3,4], O. Krause[19], R. M. Lau[20], O. Nayak[21], A. Rest[7,8], L. Colina[22], E. F. van Dishoeck[23,24], M. Güdel[19,25,26], Th. Henning[19], P.-O. Lagage[10], G. Östlin[1], T. P. Ray[4], B. Vandenbussche[27]

The nearby Supernova 1987A was accompanied by a burst of neutrino emission, which indicates that a compact object (a neutron star or black hole) was formed in the explosion. There has been no direct observation of this compact object. In this work, we observe the supernova remnant with JWST spectroscopy, finding narrow infrared emission lines of argon and sulfur. The line emission is spatially unresolved and blueshifted in velocity relative to the supernova rest frame. We interpret the lines as gas illuminated by a source of ionizing photons located close to the center of the expanding ejecta. Photoionization models show that the line ratios are consistent with ionization by a cooling neutron star or a pulsar wind nebula. The velocity shift could be evidence for a neutron star natal kick.

Supernova 1987A (SN 1987A) in the Large Magellanic Cloud is the most recent supernova (SN) in the Local Group of galaxies, so it has been extensively studied. It originated from the collapse of a blue supergiant star of 15 to 20 solar masses ($M_\odot$). Observations taken 35 years after the explosion show that the remnant of SN 1987A contains several distinct components (Fig. 1) (*1*). The inner ejecta, containing the synthesized heavy elements produced in the explosion, are now interacting with an equatorial ring (ER) and the surrounding circumstellar medium (*2*). The ER is thought to have originated ~20,000 years before the explosion, probably from a binary merger event experienced by the progenitor star (*3*, *4*). The inner ejecta produce broad emission lines with velocities of 2000 to 4000 km s^{-1}, powered by the radioactive decay of ^{44}Ti nuclei and x-rays generated by the interaction of the ejecta with the ER (*1*).

A compact object, such as a neutron star (NS) or black hole (BH), is expected to be located in the central region but has not been observed. A neutrino burst was detected coinciding with SN 1987A (*5*–*7*); its duration indicates that the compact object is probably a NS (*8*). Ionizing photons emitted by such a NS have been predicted to excite emission lines from heavy elements in the ejecta, with velocities of 100 to 1000 km s^{-1} (*9*). In this study we searched for those emission lines.

Infrared spectroscopy of SN 1987A

We observed the SN 1987A remnant on 16 July 2022 (day 12,927 after the SN explosion) using the JWST with the Mid-Infrared Instrument/Medium Resolution Spectrometer (MIRI/MRS) and the Near-Infrared Spectrograph/Integral Field Unit (NIRSpec/IFU). Both instruments produce data cubes, which contain a spectrum for each spatial pixel (*10*).

The data cubes exhibited an excess of emission in the central pixels of the ejecta (Fig. 2) at observed peak wavelengths of 4.5293 ± 0.0003 μm in the NIRSpec data and at 6.98606 ± 0.00003 μm in the MRS data, with the latter line being much brighter. We identify these as forbidden emission lines from different ionization states of ar [Ar VI] and [Ar II], which have rest wavelengt 4.52922 and 6.985274 μm, respectively. Figure 2, A to P, shows velocity slices of the MRS data cube centered on the wavelength of the [Ar II] line, and Fig. 2, Q and R, shows slices of the NIRSpec cube containing the [Ar VI] line. The [Ar II] line in SN 1987A has been observed previously (*11*), but the spatial and spectral resolution were insufficient to separate the emission from the ejecta and the ER. The JWST observations show that it arises from a central source, separated from the ER.

Figure 3A shows the [Ar II] line profile from the central source, which has a narrow strong peak and a weaker broad extension to the red. We fitted this asymmetric line profile with two Gaussian functions. Figure S2 compares the line from the center of the ejecta with the corresponding [Ar II] line from the ER. The narrow emission line component in the center is displaced by –259.6 km s^{-1} with respect to the rest frame of SN 1987A, which has a heliocentric velocity of +286.5 km s^{-1} (*12*), whereas in the spectrum of the entire ER, the [Ar II] line shows a much smaller blueshift of –12.2 ± 1.6 km s^{-1} (*10*). The velocity difference and spatial distribution indicate that the emission line from the central source is not scattered light from the ER.

The MIRI spectral resolution at the [Ar II] wavelength corresponds to a full width at half maximum (FWHM) of 87.7 ± 1.1 km s^{-1} (*13*). We measured that the narrower ejecta line component has a FWHM of 121.9 ± 1.3 km s^{-1}, so it is marginally spectrally resolved. The emission from the entire ER has a FWHM of 286 km s^{-1}, and the broader component has a value of 362.4 km s^{-1}. Table 1 lists the velocity offsets, FWHMs, and luminosities that we measured for the emission lines from the central ejecta [using a distance to SN 1987A of 49.6 kpc (*14*)].

The NIRSpec spectral resolution at the [Ar VI] 4.529-μm line is ~261 km s^{-1}. Fitting a similar two-component model as for the [Ar II] line, we found that the peak of the [Ar VI] line has consistent velocity to that of [Ar II], but the

---

[1] Department of Astronomy, Stockholm University, The Oskar Klein Centre, AlbaNova, SE-106 91 Stockholm, Sweden. [2] Department of Physics and Astronomy, University College London, London WC1E 6BT, UK. [3] Department of Experimental Physics, Maynooth University, Maynooth, County Kildare, Ireland. [4] Astronomy & Astrophysics Section, School of Cosmic Physics, Dublin Institute for Advanced Studies, Dublin 2, Ireland. [5] Department of Physics, KTH Royal Institute of Technology, The Oskar Klein Centre, AlbaNova, SE-106 91 Stockholm, Sweden. [6] UK Astronomy Technology Centre, Royal Observatory, Blackford Hill, Edinburgh EH9 3HJ, UK. [7] Space Telescope Science Institute, Baltimore, MD 21218, USA. [8] Department of Physics and Astronomy, The Johns Hopkins University, Baltimore, MD 21218, USA. [9] Jet Propulsion Laboratory, California Institute of Technology, Pasadena, CA 91109, USA. [10] Université Paris-Saclay, Université Paris Cité, Commissariat à l'Énergie Atomique et aux Énergies Alternatives, Centre National de la Recherche Scientifique, Astrophysique Instrumentation Modélisation, Saint Aubin, France. [11] Department of Astrophysical Sciences, Princeton University, Princeton, NJ 08544, USA. [12] Astronomy and Astrophysics Research Group, Department of Physics and Astrophysics, Vrije Universiteit Brussel, B-1050 Brussels, Belgium. [13] Dark Cosmology Centre, Niels Bohr Institute, University of Copenhagen, 2200 Copenhagen, Denmark. [14] Stratospheric Observatory for Infrared Astronomy Science Center, Universities Space Research Association, NASA Ames Research Center, Moffett Field, CA 94035, USA. [15] School of Physics and Astronomy, Space Research Centre, Space Park Leicester, University of Leicester, Leicester LE4 5SP, UK. [16] School of Physics and Astronomy, Cardiff University, Cardiff CF24 3AA, UK. [17] Laboratoire d'Etudes du Rayonnement et de la Matière en Astrophysique et Atmosphères, Observatoire de Paris, Paris Sciences et Lettres Research University, National Centre for Scientific Research, Sorbonne Université, Paris, France. [18] Université Paris-Saclay, Commissariat à l'Énergie Atomique et aux Énergies Alternatives, Detectors Electronics and Computing for Physics, Gif-sur-Yvette, France. [19] Max-Planck-Institut für Astronomie, D-69117 Heidelberg, Germany. [20] National Optical-Infrared Astronomy Research Laboratory, National Science Foundation, Tucson, AZ 85719, USA. [21] NASA Goddard Space Flight Center, Greenbelt, MD 20770, USA. [22] Centro de Astrobiología, Consejo Superior de Investigaciones Científicas - Instituto Nacional de Técnica Aeroespacial, Torrejón de Ardoz, E-28850, Madrid, Spain. [23] Max-Planck Institut für Extraterrestrische Physik, D-85748 Garching, Germany. [24] Leiden Observatory, 2300 RA Leiden, Netherlands. [25] Department of Astrophysics, University of Vienna, A-1180 Vienna, Austria. [26] Institute for Particle Physics and Astrophysics, Eidgenössische Technische Hochschule Zürich, 8093 Zürich, Switzerland. [27] Institute of Astronomy, Katholieke Universiteit Leuven, 3001 Leuven, Belgium.

***Corresponding author. Email: claes@astro.su.se**

†These authors contributed equally to this work.

broad components differ from the narrow blueshifted component (Table 1). Both the [Ar ɪɪ] and [Ar ᴠɪ] peaks are consistent with being spatially unresolved [the spatial resolution FWHM is 0.″350 and 0.″212 for [Ar ɪɪ] and [Ar ᴠɪ], respectively, where ″ indicates arc seconds (*10*)]. The positions of maximum emission in the [Ar ɪɪ] and [Ar ᴠɪ] lines spatially coincide (within the uncertainties) with each other and with the previously determined center of the ER (Fig. 1), which is assumed to be the explosion site (*15*).

In the MIRI data, we also detected lines of [S ɪᴠ] at 10.51 μm and [S ɪɪɪ] at 18.71 μm (fig. S3). Both sulfur lines show weak components from the central ejecta, displaced from the SN 1987A velocity by a similar amount as the argon lines. We can only place an upper limit on the luminosity of an [Ar ɪɪɪ] line at 8.991 μm (Table 1). In the NIRSpec data, we detected the [Ca ɪᴠ] line at 3.207 μm (fig. S5); however, its velocity is shifted to the red and its maximum emission is located slightly north of the [Ar ᴠɪ] peak, so it might be unrelated to the argon lines (*10*).

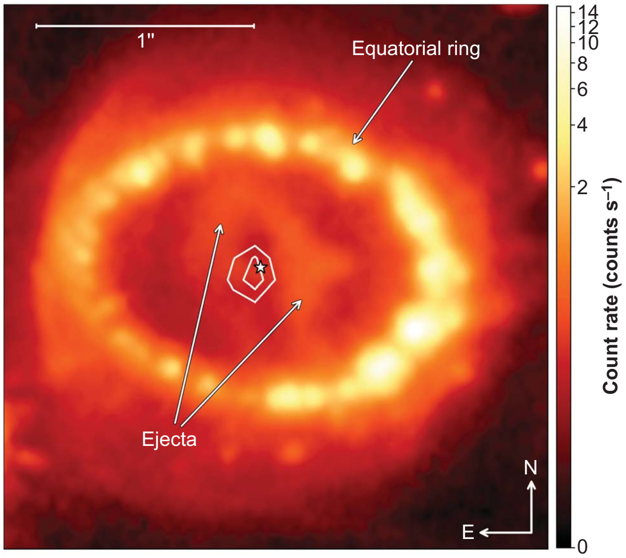

Fig. 1. Optical image of SN 1987A taken in 2022, 35 years after explosion. Hubble Space Telescope (HST) image in the F625W filter (*10*), which is dominated by Hα emission. The freely expanding inner ejecta and ER are labeled. White contours mark the [Ar ᴠɪ] 4.529-μm emission observed with NIRSpec (at 40 and 70% of the maximum surface brightness in Fig. 2S). The white star denotes the center of the ER (*15*).

Interpretation of the central emission

The only narrow emission components from the ejecta that we identified are from Ar and S, which are both produced by the nuclear burning (fusion) of O and Si. This indicates that the emission arises from the inner core of the ejecta (fig. S7). Explosion models of SN 1987A (*16*) show that the innermost ~0.07$M_\odot$ of ejecta is dominated by He and ^{56}Ni (the latter decays into ^{56}Fe). The next zone outward, with a mass of ~0.3$M_\odot$, contains material produced by oxygen burning—Si, S, Ar, Ca, and, in its outer region, also O (*10*).

The same elements have been observed in other young oxygen-rich supernova remnants (SNRs) from massive star explosions, including Cas A, SNR G54.1+0.3, and SNR 0540–69.3 (*17*–*20*) (supplementary text). Both SNR G54.1+0.3 and SNR 0540–69.3 contain pulsar wind nebulae (PWNe), powered by the spin-down power from a rapidly rotating NS with a strong magnetic field. By contrast, Cas A contains a central cooling NS (CNS) with a surface temperature $\sim 1.8 \times 10^6$ K (*21*) without a PWN. The emission lines in Cas A are mainly excited by a shock in the outer parts of the SN ejecta.

The narrow [Ar ɪɪ], [Ar ᴠɪ], [S ɪɪɪ], and [S ɪᴠ] lines that we observe from the center of SN 1987A must be excited by a source of ionizing photons or a shock wave. Potential sources include photons from a PWN generated by a NS, photons directly from a CNS, photons emitted by accretion onto a compact object, or shock excitation by a PWN shock. We also considered five other possibilities (supplementary text): ionization by radioactive ^{44}Ti; excitation produced by x-rays from the ejecta and circumstellar medium interaction; a surviving companion star; reflection of the narrow line emission from the ER collision by dust; or emission from an ingoing, reverse shock. All five possibilities were excluded.

The remaining potential explanations all include the presence of a young NS or a BH in the center. We consider a BH unlikely because the progenitor star of SN 1987A is thought to have had a total mass of $\lesssim 20M_\odot$ and an Fe core mass of $\lesssim 2M_\odot$ (*22*). The explosion ejected at least $0.07M_\odot$ of ^{56}Ni (*23*). That leaves less core mass remaining than would be required to form a BH, which is $\gtrsim 2.2M_\odot$ (*24*). Accretion of ejecta bound to the NS could be a possibility. The estimated luminosity from this, $\sim 2 \times 10^{32}$ erg s^{-1} at 35 years (*25*), is too low compared with the observed luminosity (Table 1), but the relevant physical parameters are uncertain.

A hot CNS would have a temperature of $\gtrsim 10^6$K and a luminosity of $\gtrsim 10^{34}$ergs^{-1} (*26*), which is sufficient to ionize part of the inner ejecta (*10*). An analogous case is the NS in Cas A, although it is older and fainter than what we expect for SN 1987A.

The energy loss from a pulsar is in the form of electrons, positrons, and magnetic fields, which produce an expanding high-pressure PWN. High-frequency synchrotron radiation from the relativistic particles can then ionize the ejecta

Table 1. Parameters for emission line components from the central ejecta. Luminosity calculations adopt a distance to SN 1987A of 49.6 kpc (*14*). No broad component was required for the [Ar ɪɪɪ], [S ɪᴠ], and [S ɪɪɪ] lines (fig. S3). The [Ar ᴠɪ] lines were measured in the NIRSpec data; all other lines are from the MIRI data. Uncertainties are 1σ errors on the fitting parameters; upper limits are 3σ. Dashes indicate not applicable.

Line	Wavelength (μm)	Narrow component			Broad component		
		Velocity offset (km s^{-1})	FWHM (km s^{-1})	Luminosity (10^{30} erg s^{-1})	Velocity offset (km s^{-1})	FWHM (km s^{-1})	Luminosity (10^{30} erg s^{-1})
[Ar ᴠɪ]	4.529	−269 ± 24	<377	3.04 ± 0.42	15 ± 33	<461	2.88 ± 0.40
[Ar ɪɪ]	6.985	−259.6 ± 0.4	121.9 ± 1.3	142.9 ± 2.7	−200.6 ± 3.7	362.4 ± 8.0	104.1 ± 3.0
[Ar ɪɪɪ]	8.991	–	–	<3.5	–	–	–
[S ɪᴠ]	10.510	−234 ± 12	145 ± 35	2.13 ± 0.45	–	–	–
[S ɪɪɪ]	18.713	−288 ± 13	158 ± 39	4.50 ± 0.82	–	–	–

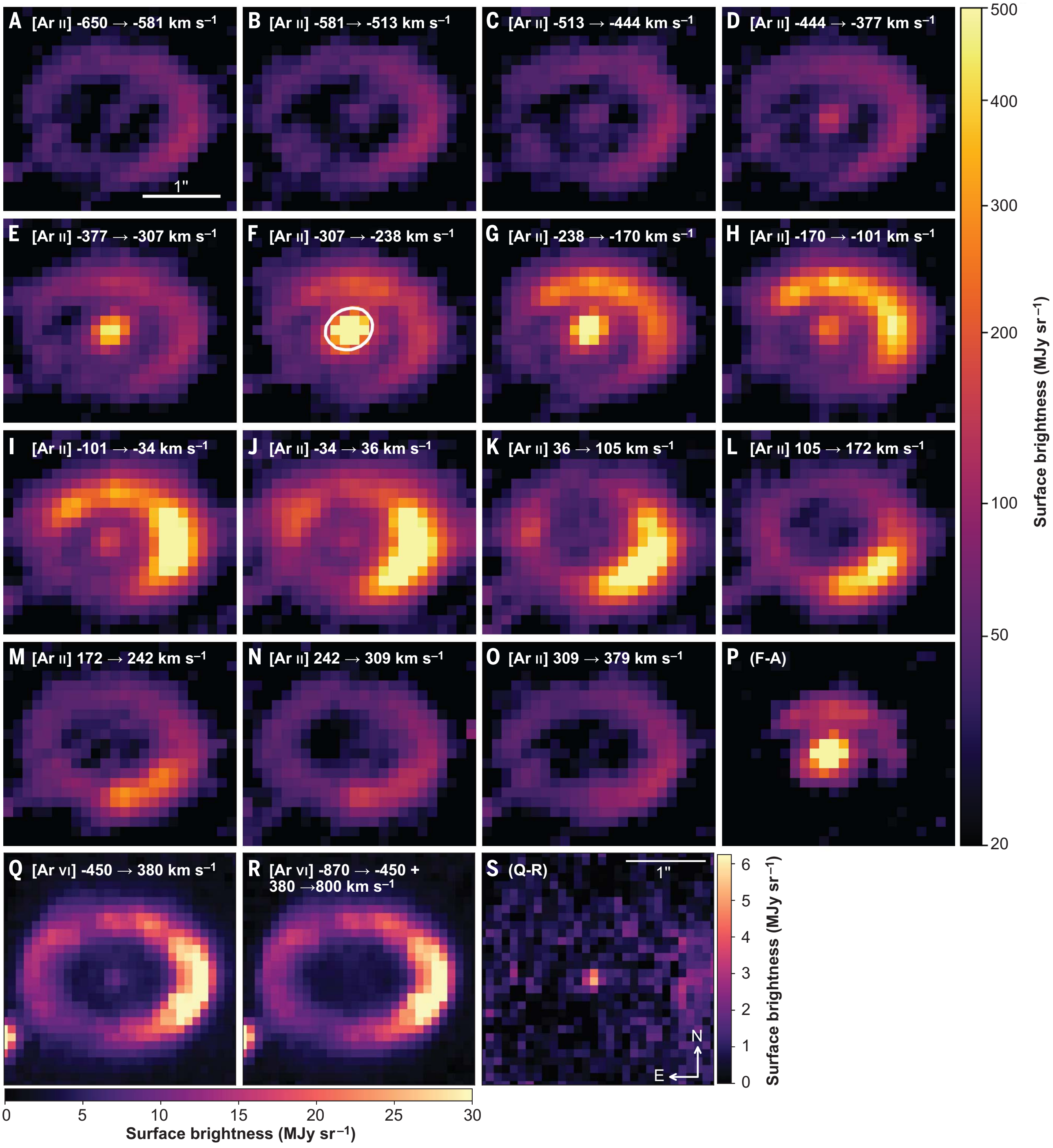

Fig. 2. JWST observations of the [Ar II] and [Ar VI] lines in SN 1987A. (**A** to **O**) Velocity slices of the MIRI/MRS data cube around the [Ar II] line at 6.985 μm. Labels in each panel indicate the corresponding velocity ranges, measured with respect to the systemic velocity of SN 1987A (*12*). Emission is apparent from a central source, which has its maximum intensity offset in velocity from the ER by ~−250 km s^{-1}. The white circle in (F) indicates the region used to extract the spectrum in Fig. 3A. (**P**) Residuals between (F) and (A). (**Q**) NIRSpec observations of the [Ar VI] 4.529-μm line, combining all velocity slices between −450 and +380 km s^{-1}. (**R**) The NIRSpec data stacked outside that velocity range. (**S**) Residuals between (Q) and (R), separating the emission from the central source. The bright point in the lower left areas of (Q) and (R) is an unrelated star. Color bars are in units of megajansky (MJy) per steradian.

(*9*). The luminosities and spectra of the PWNs discussed above are not consistent with the bolometric and monochromatic luminosity of the SN 1987A remnant, whereas a slowly rotating and/or weakly magnetized NS is compatible with the observations (*15*). We expect an expanding PWN bubble to sweep up a dense shell of ejecta, separated from the PWN by a shock, which could also excite the lines that we observed. The velocity of the dense shell would depend on the energy input from the pulsar along with the density and expansion velocity of the ejecta (*9*). These parameters are all uncertain, but estimates for SN 1987A produce a shell velocity of 150

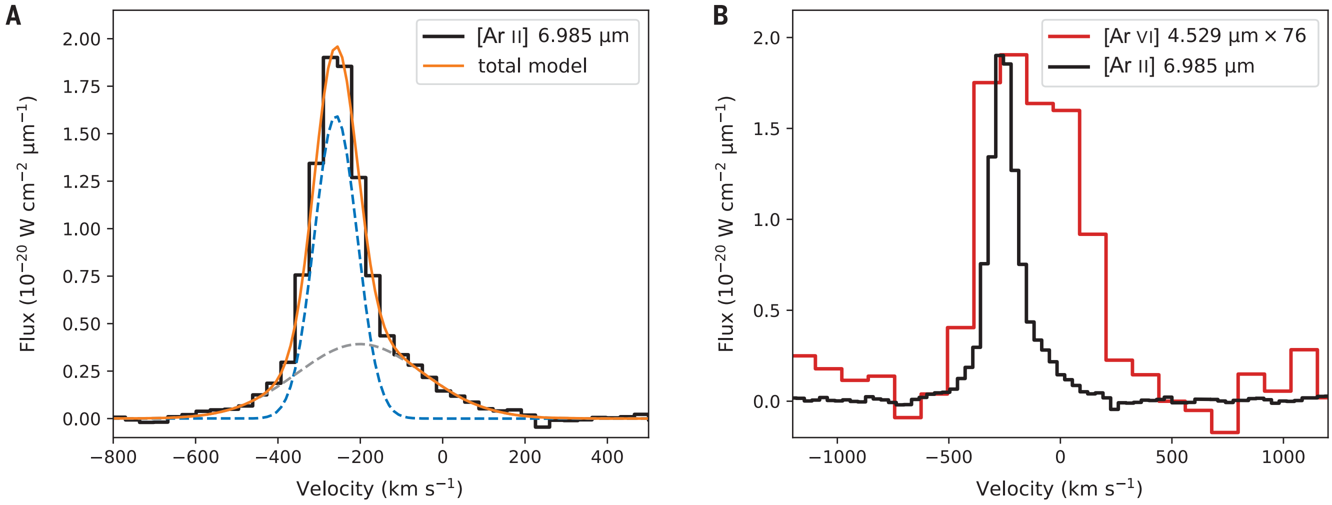

Fig. 3. Velocity profiles of the [Ar II] 6.985-µm and [Ar VI] 4.529-µm lines from the central source. (**A**) The [Ar II] line in the MRS data (black histogram) extracted from the region indicated in Fig. 2F. The orange curve is a model fitted to the data, consisting of two Gaussian components (blue and gray dashed curves). (**B**) The same [Ar II] data (black histogram), compared with the [Ar VI] line from the NIRSpec data (red histogram). The [Ar VI] data have a lower spectral resolution and have been scaled by a factor of 76 for display.

to 300 km s^{-1} and a PWN shock velocity of 30 to 50 km s^{-1} (*10*).

Photoionization models

To investigate these interpretations in more detail, we updated a photoionization modeling code (*9*) and applied it to the PWN and CNS scenarios (*10*). The resulting emission line spectrum is primarily determined by the ionization parameter $\xi = L_{\rm ion}/n_{\rm ion}r^2$, where $L_{\rm ion}$ is the ionizing luminosity, $n_{\rm ion}$ is the number density of ions, and r is the distance to the ionizing source; it is affected to a lesser extent by the spectral form of the luminosity $L(\nu)$, where ν is the frequency (*10*). For the ionizing spectrum of a PWN, we assume a power law $L(\nu) \propto \nu^{-\alpha}$, with $\alpha = 1.1$. This matches the ultraviolet–to–x-ray spectrum of the Crab Nebula (*27*) and is within the range of $0.5 < \alpha < 1.1$ previously found for x-rays in young PWNs (*28*, *29*). We also investigated using steeper power laws and found that it has little effect (supplementary text). Previous work has constrained $L_{\rm ion} \lesssim 10^{36}$ erg s^{-1} at energies above 13.6 eV (*15*).

For the young CNS scenario, previous models have found an upper limit to the thermal luminosity of $\lesssim 4 \times 10^{35}$ erg s^{-1} and a surface temperature of ~(1.5 to 3) × 10^6 K at 35 years after the explosion (*26*, *30*, *31*). Central compact objects, like the NS in Cas A, are thought to have carbon-dominated atmospheres (*21*), although alternative models producing a hard spectrum have been discussed (*32*). We adopted a carbon-dominated CNS spectrum (*21*) and set $L_{\rm ion} = 3 \times 10^{35}$ erg s^{-1}.

The models depend on the density in the ejecta core, which is uncertain. After explosion, the mass inside the oxygen core of a $19-M_\odot$ progenitor is $\sim 3.0 M_\odot$, after excluding the material that forms the NS (*16*). The line profiles indicate a core velocity of ~2200 km s^{-1} (*10*). For a uniform core density, $n_{\rm ion} \approx 2.6 \times 10^3$ $(A/22)^{-1}$ cm^{-3} after 35 years, where A is the mean atomic weight in the O-Si-S-Ar core. However, both observations (*33*–*36*) and simulations (*37*) indicate that clumping and filaments produce regions with higher densities in this zone, whereas Fe-rich regions can have lower density as a result of early heating by decay of ^{56}Ni (*10*). If a PWN is present, it produces a dense shell (as discussed above), which is likely to be unstable and clumpy (*9*, *38*). We therefore assume a density of $n_{\rm ion} = 2.6 \times 10^4$ cm^{-3}, which is 10 times the average estimated above, in both models.

Figure 4 shows the lines predicted by the models of the PWN and CNS scenarios for an ejecta composition (fig. S7) typical of explosive oxygen burning in a SN with a $19-M_\odot$ progenitor star (*10*, *16*). The blueshifted line velocities and dust effects indicate that only a fraction of the total ionizing luminosity is converted to the observed emission lines (supplementary text). We therefore normalized the [Ar II] luminosity by a covering factor, chosen to match the observed luminosity, and scaled the other lines to their relative model luminosities (*10*). For consistency, we included only the luminosities of the blueshifted narrow component.

The relative luminosities of the [Ar II] 6.985-µm and [Ar VI] 4.529-µm lines are reproduced in both models (Fig. 4), with this assumed density and $\xi \approx 0.3$ (*10*). Both models predicted other high-ionization emission lines, including [Ca IV] 3.207-µm, [Ca V] 4.159-µm, [Ar V] 7.902-µm, [Ar III] 8.991-µm, [S IV] 10.51-µm, [Ar V] 13.10-µm, [S III] 18.71-µm, [Ar III] 21.83-µm, [O IV] 25.89-µm, and [Fe II] 25.99-µm lines (Fig. 4). Most of these lines have previously been observed in young, oxygen-rich SNRs (supplementary text). However, in SN 1987A, the lines at wavelengths higher than ~8 µm are much weaker than predicted (relative to the [Ar II] line) or are absent entirely, although we do detect faint emission for [S IV] 10.51-µm and [S III] 18.71-µm lines (fig. S3).

Dust effects on the observed emission

Infrared observations have shown that a large amount of dust was formed in the ejecta of SN 1987A (*39*, *40*), consisting of a mixture of grains composed of silicates and graphite (*41*, *42*). However, the composition of the dust close to the center is likely to differ from that of the outer regions (*10*). Dust nucleation models have predicted that silicates dominate over carbon-rich dust in the central regions (*43*–*46*), of which Mg_2SiO_4 (forsterite) is expected to have the highest abundance. Observations of young SNRs have shown that silicates are the dominant type of dust (*10*).

Silicate dust grains strongly absorb wavelengths longer than ~8 µm (fig. S8). This is a potential explanation for why we do not detect the long-wavelength lines at the luminosities predicted by the photoionization models.

We are unable to estimate the optical depth $\tau_{\rm abs}$ at those wavelengths because of the unknown dust composition, grain size, and clumping. However, $\tau_{\rm abs}$ is likely to be large (*47*). Figure 4 also shows the dust absorption expected for an assumed optical depth of $\tau_{\rm abs} = 6.5$ at 10 µm and amorphous forsterite composition (*48*) and the line luminosities after including this dust absorption. Although the predicted luminosities of lines shorter than ~8 µm are only slightly affected, those at longer wavelengths are substantially suppressed. For [S IV] 10.51-µm and [S III] 18.71-µm lines, this correction brings the model predictions close to the observed line

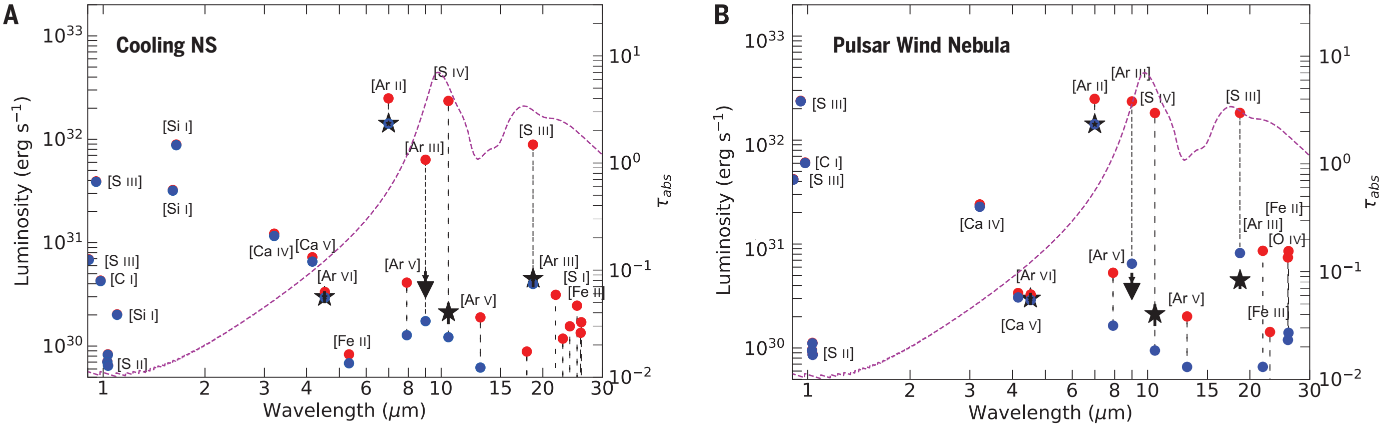

Fig. 4. Photoionization models compared with observed lines. (**A**) Model of the oxygen-burning layers expected in a SN ionized by a young CNS. (**B**) Model of the same material ionized by a PWN. The optical depth due to silicate dust (magenta curve, on the right axis) assumes Mg$_2$SiO$_4$ composition and τ_{abs} = 6.5 at 10 μm in both cases. Circles show the model-predicted line luminosities (left axis) before (red) and after (blue) including dust absorption, which are connected by dashed vertical lines. Line identifications are labeled near each red circle. Black stars are the observed luminosities (Table 1) for the [S III], [S IV], [Ar II], and [Ar VI] lines, with error bars showing 1σ uncertainties, which are mostly smaller than the symbol size. The upper limit for the [Ar III] line (black triangle) is 3σ.

luminosities. The observed upper limit on the [Ar III] 8.991-μm line is consistent with the model.

The CNS model (Fig. 4A) predicts strong [Si I] lines at 1.607 and 1.645 μm. These are not detected in our observations, perhaps because they are blended with broad lines from the ejecta. Dust scattering, dust depletion, and ionization of silicon by the ultraviolet flux from the ejecta and ring could all reduce the predicted luminosities of these lines (*10*).

We have also modeled the expected line luminosities from a PWN shock (*10*). Most of the observed lines are reproduced (supplementary text) (fig. S12) without requiring dust absorption. However, the [S III] 18.71-μm line is underproduced by a factor of ~25.

The nature of the compact object

Given the uncertain model assumptions about the ionizing spectrum, density, elemental abundances, and dust properties, we conclude that the observed lines can be explained by either the CNS or PWN photoionization models. Both require the presence of a NS. Because thermal emission from the CNS should always be present at some level, a combination of both models is also possible. For the model parameters adopted above, the PWN shock scenario is less likely but not excluded (*10*).

There have been previous indications of emission from a central object in SN 1987A. Submillimeter dust maps of the ejecta show a peak in the temperature close to the central region, which might be due to extra energy input from a central source (*47*). The peak temperature position does not coincide with the location of maximum [Ar VI] emission in our observations (*10*); however, this does not rule out additional heating from a compact object (*31*). X-ray observations of SN 1987A have detected nonthermal emission at energies above 10 keV, which has been interpreted as being due to a central source (*49*, *50*); this would support the PWN scenario. However, the same observations have alternatively been interpreted as thermal emission from the shocks in the ER (*51*).

The position and velocity of the argon emission lines constrain any natal kick—a velocity imparted on the NS during its formation by anisotropies in the explosion mechanism. The offset in position of the narrow emission components corresponds to a velocity 416 ± 206 km s^{-1} given the time since the explosion (supplementary text). However, converting this to a kick velocity depends on the separation between the NS and the line-emitting region, which differs between the CNS and PWN models.

Our observations of high-ionization emission lines in the center of the SN 1987A remnant indicate the presence of a source of ionizing photons, probably a NS. We cannot determine which scenario is more likely—young CNS or PWN—but both require the presence of a NS.

REFERENCES AND NOTES

1. R. McCray, C. Fransson, *Annu. Rev. Astron. Astrophys.* **54**, 19–52 (2016).
2. J. Larsson *et al.*, *Astrophys. J. Lett.* **949**, L27 (2023).
3. T. Morris, P. Podsiadlowski, *Science* **315**, 1103–1106 (2007).
4. T. Morris, P. Podsiadlowski, *Mon. Not. R. Astron. Soc.* **399**, 515–538 (2009).
5. E. N. Alekseev, L. N. Alekseeva, V. I. Volchenko, I. V. Krivosheina, *JETP Lett.* **45**, 589–592 (1987).
6. R. M. Bionta *et al.*, *Phys. Rev. Lett.* **58**, 1494–1496 (1987).
7. K. Hirata *et al.*, *Phys. Rev. Lett.* **58**, 1490–1493 (1987).
8. A. Burrows, *Astrophys. J.* **334**, 891 (1988).
9. R. A. Chevalier, C. Fransson, *Astrophys. J.* **395**, 540 (1992).
10. Materials and methods are available as supplementary materials.
11. R. G. Arendt *et al.*, *Astron. J.* **151**, 62 (2016).
12. P. Gröningsson *et al.*, *Astron. Astrophys.* **492**, 481–491 (2008).
13. O. C. Jones *et al.*, *Mon. Not. R. Astron. Soc.* **523**, 1297–1309 (2023).
14. G. Pietrzyński *et al.*, *Nature* **567**, 200–203 (2019).
15. D. Alp *et al.*, *Astrophys. J.* **864**, 174 (2018).
16. S. E. Woosley, A. Heger, *Phys. Rep.* **442**, 269–283 (2007).
17. R. A. Chevalier, R. P. Kirshner, *Astrophys. J.* **233**, 154 (1979).
18. J. D. T. Smith *et al.*, *Astrophys. J.* **693**, 713–721 (2009).
19. T. Temim, P. Slane, S. P. Reynolds, J. C. Raymond, K. J. Borkowski, *Astrophys. J.* **710**, 309–324 (2010).
20. B. J. Williams *et al.*, *Astrophys. J.* **687**, 1054–1069 (2008).
21. W. C. G. Ho, C. O. Heinke, *Nature* **462**, 71–73 (2009).
22. T. Sukhbold, S. E. Woosley, A. Heger, *Astrophys. J.* **860**, 93 (2018).
23. P. Bouchet *et al.*, *Astron. Astrophys.* **245**, 490–498 (1991).
24. C. Musolino, C. Ecker, L. Rezzolla, On the maximum mass and oblateness of rotating neutron stars with generic equations of state. arXiv:2307.03225 [gr-qc] (2023).
25. R. A. Chevalier, *Phys. Rep.* **256**, 95–108 (1995).
26. M. V. Beznogov, A. Y. Potekhin, D. G. Yakovlev, *Phys. Rep.* **919**, 1–68 (2021).
27. M. Lyutikov *et al.*, *Mon. Not. R. Astron. Soc.* **489**, 2403–2416 (2019).
28. X.-H. Li, F.-J. Lu, Z. Li, *Astrophys. J.* **682**, 1166–1176 (2008).
29. E. V. Gotthelf, *Astrophys. J.* **591**, 361–365 (2003).
30. M. V. Beznogov, J. Novak, D. Page, A. R. Raduta, *Astrophys. J.* **942**, 72 (2023).
31. D. Page *et al.*, *Astrophys. J.* **898**, 125 (2020).
32. J. A. J. Alford, J. P. Halpern, *Astrophys. J.* **944**, 36 (2023).
33. J. Spyromilio, P. A. Pinto, *European Southern Observatory Conference and Workshop Proceedings, Vol. 37, Supernova 1987A and Other Supernovae*, I. J. Danziger, K. Kjär, Eds. (European Southern Observatory, 1991), p. 423.
34. H. Li, R. McCray, *Astrophys. J.* **387**, 309 (1992).
35. J. Larsson *et al.*, *Astrophys. J.* **768**, 89 (2013).
36. M. Matsuura *et al.*, *Mon. Not. R. Astron. Soc.* **469**, 3347–3362 (2017).
37. M. Gabler, A. Wongwathanarat, H.-T. Janka, *Mon. Not. R. Astron. Soc.* **502**, 3264–3293 (2021).
38. J. M. Blondin, R. A. Chevalier, *Astrophys. J.* **845**, 139 (2017).
39. D. H. Wooden *et al.*, *Astrophys. J. Suppl. Ser.* **88**, 477 (1993).
40. M. Matsuura *et al.*, *Science* **333**, 1258–1261 (2011).
41. M. Matsuura *et al.*, *Astrophys. J.* **800**, 50 (2015).
42. R. Wesson, M. J. Barlow, M. Matsuura, B. Ercolano, *Mon. Not. R. Astron. Soc.* **446**, 2089–2101 (2015).
43. A. Sarangi, I. Cherchneff, *Astron. Astrophys.* **575**, A95 (2015).
44. A. Sarangi, M. Matsuura, E. R. Micelotta, *Space Sci. Rev.* **214**, 63 (2018).
45. A. Sluder, M. Milosavljević, M. H. Montgomery, *Mon. Not. R. Astron. Soc.* **480**, 5580–5624 (2018).
46. A. Sarangi, *Astron. Astrophys.* **668**, A57 (2022).

47. P. Cigan *et al.*, *Astrophys. J.* **886**, 51 (2019).
48. H.-P. Gail, A. Tamanai, A. Pucci, R. Dohmen, *Astron. Astrophys.* **644**, A139 (2020).
49. E. Greco *et al.*, *Astrophys. J. Lett.* **908**, L45 (2021).
50. E. Greco *et al.*, *Astrophys. J.* **931**, 132 (2022).
51. D. Alp, J. Larsson, C. Fransson, *Astrophys. J.* **916**, 76 (2021).
52. O. Jones, SN1987A MRS Spectralcube (Mikulski Archive for Space Telescopes, 2023); https://doi.org/10.17909/pz4v-ej33.
53. J. Larsson, JWST NIRSpec SN 1987A (Mikulski Archive for Space Telescopes, 2023); https://doi.org/10.17909/175h-7x33.
54. P. Kavangh, Data used in paper (Mikulski Archive for Space Telescopes, 2023); https://doi.org/10.17909/7an5-yp54.
55. J. Larsson, HST/WFC3 F625W & F657N, 2022, SN 1987A (Mikulski Archive for Space Telescopes, 2023); https://doi.org/10.17909/53qa-pd67.
56. C. Fransson, P. Kavanagh, claesob/SN-codes: Updated release, version 2.5, Zenodo (2024); https://doi.org/10.5281/zenodo.10476657.
57. C. Fransson, claesob/SN87A_shock: Updated release, version 1.5, Zenodo (2024); https://doi.org/10.5281/zenodo.10476710.

ACKNOWLEDGMENTS

We thank R. Chevalier, T. Janka, S. Woosley, and the anonymous referees for constructive comments on the paper and useful discussions. MIRI development was supported by NASA, the European Space Agency (ESA), the Belgian Science Policy Office (BELSPO), the Centre Nationale d'Etudes Spatiales (CNES), the Danish National Space Centre, Deutsches Zentrum fur Luft-und Raumfahrt (DLR), Enterprise Ireland, Ministerio De Economiá y Competividad, the Netherlands Research School for Astronomy (NOVA), the Netherlands Organisation for Scientific Research (NWO), the Science and Technology Facilities Council, the Swiss Space Office, the Swedish National Space Agency, and the UK Space Agency. This study is based on observations made with the NASA/ESA/CSA JWST. The data were obtained from the Mikulski Archive for Space Telescopes at the Space Telescope Science Institute, which is operated by the Association of Universities for Research in Astronomy, Inc., under NASA contract no. NAS 5-03127 for JWST. **Funding:** C.F., J.L., and G.Ö. acknowledge support from the Swedish National Space Agency. J.L. acknowledges support from the Knut and Alice Wallenberg Foundation. M.J.B. acknowledges support from European Research Council advanced grant ERC-2015-AdG-694520-SNDUST. P.J.K. and J.J. acknowledge support from Science Foundation Ireland/Irish Research Council Pathway program under grant no. 21/PATH-S/9360. O.C.J. acknowledges support from an STFC Webb fellowship. M.M. and N.H. acknowledge support through NASA/JWST grant 80NSSC22K0025. M.M. and L.L. acknowledge support from the NSF through grant 2054178. J.H. was supported by a VILLUM FONDEN Investigator grant, project no. 16599. O.N. acknowledges support from STScI Director's Discretionary Fund. T.Ti. acknowledges financial support from the UK Science and Technology Facilities Council and the UK Space Agency. Part of the research of M.M. and N.H. was carried out at the Jet Propulsion Laboratory, California Institute of Technology, under a contract with NASA (80NM0018D0004). L.C. acknowledges support by grant PIB2021-127718NB-100 from the Spanish Ministry of Science and Innovation/State Agency of Research MCIN/AEI/10.13039/501100011033. J.A.D.L.B. and B.V. thank BELSPO for the provision of financial support in the framework of the PRODEX Programme of the ESA. **Author contributions:** C.F. led the project, performed the modeling, wrote most of the text, and contributed to the data analysis. M.J.B. and P.B. wrote the proposal science case, designed the observations, and coordinated the SN 1987A Guaranteed Time Observations (GTO) program no. 1232. P.J.K. performed the MIRI MRS data reduction. M.J.B., P.J.K., and J.L. contributed to the data analysis and writing. O.C.J. designed the observations and was the science lead for the SN 1987A observations program. B.S. performed the NIRSpec data reduction. M.M. is the co–primary investigator (co-PI) of the SN 1987A observations program, provided 3 of the 9 hours of GTO time used for the observations, and contributed to the data analysis. T.Te. contributed to the interpretation of the data. A.S.H. optimized the observational program. N.H. and A.R. assisted with data processing. A.C., A.G., J.A.D.L.B., J.H., J.J., L.L., O.K., O.N., O.D.F., R.G., R.M.L., R.W., and T.Ti. commented on the manuscript. G.S.W., L.C., E.F.v.D., M.G., Th.H., P.-O.L., G.Ö., T.P.R., and B.V. are MIRI PIs and co-PIs, who also commented on the manuscript. **Competing interests:** The authors declare that they have no competing interests. **Data and materials availability:** The observations are available at the Mikulski Archive for Space Telescopes (https://mast.stsci.edu/) under proposal IDs 1232 and 1524 for JWST and 16789 for HST. The specific MRS and NIRSpec SN 1987A observations that we used are archived (*52*, *53*) as are the 10 Lac observation used for calibration (*54*) and the HST observation (*55*). The source code used for the PWN and CNS models is available at https://github.com/claesob/SN-codes and archived at Zenodo (*56*). The source code for the shock models is available at https://github.com/claesob/SN87A_shock and archived at Zenodo (*57*). **License information:** Copyright © 2024 the authors, some rights reserved; exclusive licensee American Association for the Advancement of Science. No claim to original US government works. https://www.science.org/about/science-licenses-journal-article-reuse

SUPPLEMENTARY MATERIALS

science.org/doi/10.1126/science.adj5796
Materials and Methods
Supplementary Text
Figs. S1 to S12
Tables S1 to S3
References (*58–125*)

Submitted 6 July 2023; accepted 12 January 2024
10.1126/science.adj5796